A moderately chocked estuary: Influence of a constriction on the water level variations of the Wouri estuary (Cameroon)

Willy Noël Dima, Yves Morel, Vanessa Elvire Toukep Ngnepi, Raphael Onguene, Thomas Stieglitz, Thomas Duhaut, Bénédicte Lemieux-Dudon, Jules Romain Ngueguim, Felix Besack, Ezinvi Baloitcha, et al.

A moderately chocked estuary: Influence of a constriction on the water level variations of the Wouri estuary (Cameroon)

Willy Noël DIMA [*, a, c], Yves MOREL [b, f], Vanessa Elvire TOUKEP NGNEPI [d], Raphael ONGUENE [d], Thomas STIEGLITZ [e], Thomas DUHAUT [b], Bénédicte LEMIEUX-DUDON [b], Jules Romain NGUEGUIM [a], Felix BESACK [g], Ezinvi BALOITCHA[c], Alexis CHAIGNEAU [b].

[*] Corresponding authors

Email addresses: willy.dimamccoy@gmail.com (Willy Noel Dima), yves.morel@univ-tlse3.fr (Yves Morel), ngnepivanessa@yahoo.fr (Vanessa Elvire Toupek Ngnepi), ziongra@yahoo.fr (Raphael Onguene), stieglitz@cerege.fr (Thomas Stieglitz), thomas.duhaut@univ-tlse3.fr (Thomas Duhaut), lemieux.benedicte@gmail.com (Bénédicte Lemieux-Dudon), njules_romain@hotmail.com (Jules Romain Ngueguim), besackocean@gmail.com (Felix Besack), ezinvi.baloitcha@gmail.com (Ezinvi Baloitcha) alexis.chaigneau@ird.fr (Alexis Chaigneau)

[a] Specialized Research Station on Marine Ecosystems (SS-ECOMA), IRAD - Kribi, Cameroon

[b] LEGOS, University of Toulouse, CNES, CNRS, IRD, UT3, Toulouse, France

[c] International Chair in Mathematical Physics and Applications (ICMPA, UNESCO Chair)/University of Abomey-Calavi, Cotonou, Benin

[d] University of Douala, Laboratoire de Technologie et Sciences Appliquées (LTSA-Douala), Cameroon

[e] Aix-Marseille Université, CNRS, IRD, INRAE, Coll France, CEREGE, Aix-en- Provence, France

[f] LOPS, University of Brest, CNRS, IRD, Ifremer, IUEM, France

[g] Department of oceanography of the Institute of Fisheries and Aquatic Sciences of the University of Douala, Association for the Conservation of Nature (Ascon), Cameroon

Abstract

The study focuses on the evolution of water levels (WL) in the Douala basin, a sub-basin of the Wouri estuary, separated from the open ocean by a natural constriction and influenced by tides and river inflow. Our objective is to assess whether floods in the adjacent coastal city of Douala could result from water overflow from the Douala basin due to Wouri river floods.

We first evaluate the constriction's damping effect by analyzing the tide amplitude variations from the ocean to the basin. We develop a simplified model for the variation in basin WL, which includes a dissipation parameter, that is evaluated using the weak modulation of tidal amplitudes from the ocean to the basin over the dry season of 2023. Our findings indicate a moderate level of dissipation in the constriction.

Subsequently, the model is used to evaluate the mean and maximum WL, as well as tide amplitude variations of the Doula basin, as functions of river flow and ocean tides. The mean WL increases, but the maximum tide amplitude decreases as river input increases. The maximum WL in the basin always exceeds the maximum amplitude of ocean tides but is only significantly higher when river input is above 1000 m^3/s.

In current conditions, where maximum observed river input is around 1800 m^3/s, it is unlikely that flooding will extend beyond the basin borders into the city of Douala. For a moderate increase (20%) in future maximum river fluxes, it is also unlikely that the Douala basin will overflow into Douala city. Only a drastic increase in mean ocean level and river fluxes (which are possible scenarios associated with climate change) could potentially lead to a significant rise in basin WL, resulting in severe flooding.

Key words: estuary, water level, tide, river flow, Douala.

1. Introduction

Estuaries and lagoons are complex transitional systems where seawater mixes with fresh water (e.g. Duck and da Silva, 2012). They are often described as interfaces between oceans

and continents, and are considered among the world's most productive ecosystems. They play a critical role in biodiversity, serving as important habitats, spawning grounds and feeding areas for numerous marine or aquatic species (Harley et al.,2006; Scanes et al.,2020; Maicu et al., 2021). Due to these characteristics, these areas provide significant economic benefits for several human activities such as fishing, aquaculture, sand extraction or tourism (e.g., Gonenc and Wolflin, 2004; Umgiesser et al., 2014; Newton et al., 2018).

Transitional waters are highly responsive to changes in external forcing, leading to significant spatio-temporal fluctuations of physical, biogeochemical or biological variables (Viaroli et al., 2007; Tagliapietra et al., 2009; Barbone and Basset, 2010; Umgiesser et al., 2014). In recent years, flooding has become one of the main causes of natural disasters worldwide (Paprotny et al., 2018). Urban flooding risks are increasing due to rapid urbanization and climate change in many cities globally, both in coastal and continental settings (Abebe et al., 2018). Although there are uncertainties regarding the evolution of precipitation patterns associated with climate change, this trend is likely to persist or intensify in the future (Bertoni, 2006; Stocker, 2014). Sub-Saharan Africa is a region where the risks associated with global change, including climate change and anthropogenic pressure, are particularly significant (Martinis, 2017; Hu et al., 2019). In Cameroon, the Wouri estuary experiences high flow conditions during the rainy season (May-October) and low flow conditions during the dry season (November to April) (Olivry, 1974). Flash floods, i.e. sudden increases in water level (WL), can have dramatic consequences for local populations. Since the 1980s, the coastal city of Douala has experienced unplanned urban expansion, driven by rural migration. The large influx of people has resulted in settlement of areas identified as flood-prone zones, swamps, and mangroves, increasing their vulnerability. Between 1980 and 2018, Douala experienced 34 major floods (Amanejieu, 2018), resulting in more than 100 deaths and significant damage between 2000 and 2010 (Bruckmann et al., 2019). This underlines the importance of implementing flood warning systems to protect both the population and properties. To do so, a scientific analysis of the causes of recorded floods is necessary. We here assess the potential impact of ocean surge (or more accurately, basin surge) on the flood risk of the city.

In estuaries or lagoons, WL are primarily influenced by ocean waves and tides, river inputs, the wind and, to a lesser extent, direct precipitation contributions (e.g., Chaigneau et al., 2022; Albrecht and Vennell, 2007). Waves associated with storm surges can play a crucial role in coastal flooding, especially when they coincide with high tides and/or river flooding (Zheng

et al., 2013). However, the Douala basin is located in the upper part of the estuary and is protected from the intrusion of large amplitude waves (Besack et al., 2020).

Observations indeed highlight that floods in Douala city follow periods of intense precipitation and become almost annual, more intense, and more severe along the Wouri river (Munji et al., 2014). The interaction between tides and river flow can play a major role on the WL variations in an estuary or lagoon and depends on dissipation associated with bottom friction (Stigebrandt, 1980; Speer, 1985). While tidal amplitude can increase in converging estuaries, dissipation along channels, or constrictions connecting the ocean to an inland basin or lagoon, reduces the tidal amplitude while increasing river WL during flood periods (Stigebrandt, 1980; Glenne and Simensen, 1963; Oliveira and Kjerfve, 1993; Hill, 1994; Buschman et al., 2009; Sassi and Hoitink, 2013). Recently, it has been shown that the nonlinear interaction of tides, river flow, and friction can influences the seasonal WL variability when the dissipation and river flow are high (Morel et al., 2022) and that these processes should be considered when predicting WL variations across different temporal scales.

The city of Douala is located adjacent to a small sub-basin of the Wouri estuary, referred as the Douala basin. This basin is separated from the ocean by a constriction across which two bridges have been constructed, potentially increasing dissipative effects. Recent observations within the Wouri estuary (Besack et al., 2020 ; Fossi Fotsi et al., 2023) have indeed shown that tide amplitude is damped in the Douala basin in comparison with the ocean. However the damping remain moderate and is sensitive to both tide amplitude and season (that is to say river flow).The objective of this study is to determine whether WL variations in the Douala basin could lead to flooding in the city of Douala, either presently or in the future. We focus on the interaction of river flow and ocean tide. We use a model, based on Stigebrandt (1980) (see also Hill, 1994; Albrecht and Vennell, 2007; MacMahan et al., 2014; Morel et al., 2022), which relies on the estimation of a dissipation coefficient Γ. We propose a method to estimate Γ by observing tide modulation in the Douala basin. We present a new set of analytical solutions for the Stigebrandt (1980) model, applicable under moderate dissipation. This allows us to evaluate the dissipation parameter relative to the constriction. Subsequently, the model is validated using available data and used to estimate mean WL, tide amplitude and maximum WL in the Douala basin, depending on river flow and ocean tides.

2. Geographical context, data and model

2.1. *Douala basin (DB)*

The Wouri estuary flows into the Atlantic on the central coast of Cameroon (Fig. 1-B). Our focus in this study is the upper part of the estuary (Fig. 1-C), an area that forms a basin near Douala. The lower estuary is wide and can be considered part of the ocean. The DB covers approximately 9 km^2. It is separated from the ocean by a constriction approximately 1000-m long and 400-m wide, resembling a channel. The depth of this constriction varies significantly, reaching depths of more than 10 m (Fig. 1-C). Additionally, the constriction is crossed by two bridges with pylons than can locally impact bathymetry and flow. Thus, dissipation can be expected, leading to an elevation of the mean WL in the basin, potentially causing flooding in districts bordering the DB. This is the hypothesis we aim to investigate in this study.

We observed WL variations at three locations, positioned on both sides of the constriction (Fig. 1-C). Two sensors are located within the DB and one is located at the Port of Douala, representing oceanic WL variations primarily associated with tides. These oceanic variations act as a forcing condition for the DB.

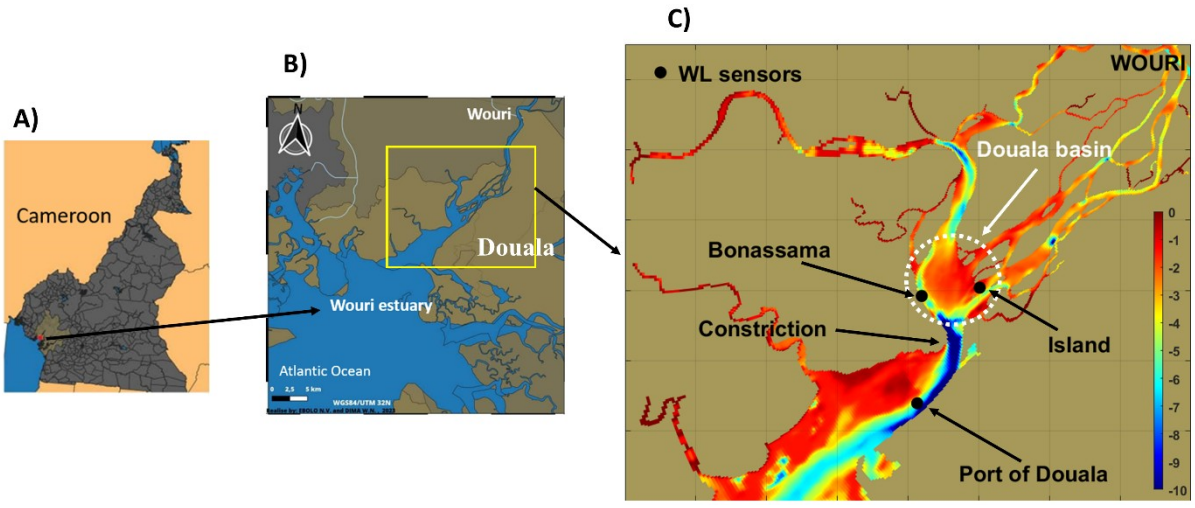

Fig. 1. Geographical location of the Wouri estuary. A: Map of Cameroon. B: Map of the Wouri estuary. C: Bathymetry of the upper part of the estuary where the Douala basin is located. The black dots correspond to the positions of the water-level sensors used in this study.

2.2. *WL variations in the DB*

WL data were recorded by two pressure sensors deployed near the constriction zone. These observations span two distinct periods: the first period extends from March to December 2022 for the sensor deployed at Bonassama, and the second period from February to early April 2023 for the sensor deployed near an island in the middle of the basin (see Fig. 1C). Each station was equipped with a HOBO Onset WL Logger P/N: U20L-01 anchored 20-30 cm from the bottom in a PVC tube with an external diameter of 7 cm and perforated over its whole length. Data were recorded continuously at one-hour intervals for each tide gauge, with a typical accuracy of ±1 cm and a maximum error of 2 cm (Wilson et al., 2016; Guragai et al., 2018; Chaigneau et al., 2021).

The observed variations are influenced by both oceanic tides and the river's hydrology (Fig 2). The short observation period for the" Island sensor" falls within the dry season when Wouri river flow is minimal (see section 2.4 below). The vertical reference is here chosen to be the mean WL over the observation period.

For the available data at Bonassama, the observations span nearly a year, including the wet season when river fluxes reach their maximum values. The available data are truncated and do not cover the entire tide cycle, because the sensor was positioned in an area that falls dry during low tides for accessibility and security reasons. However, these data can still be used for model validation. In this case, the vertical reference is established at the minimum pressure recorded by the sensor. The impact of atmospheric pressure variations is clearly noticeable at low pressure levels.

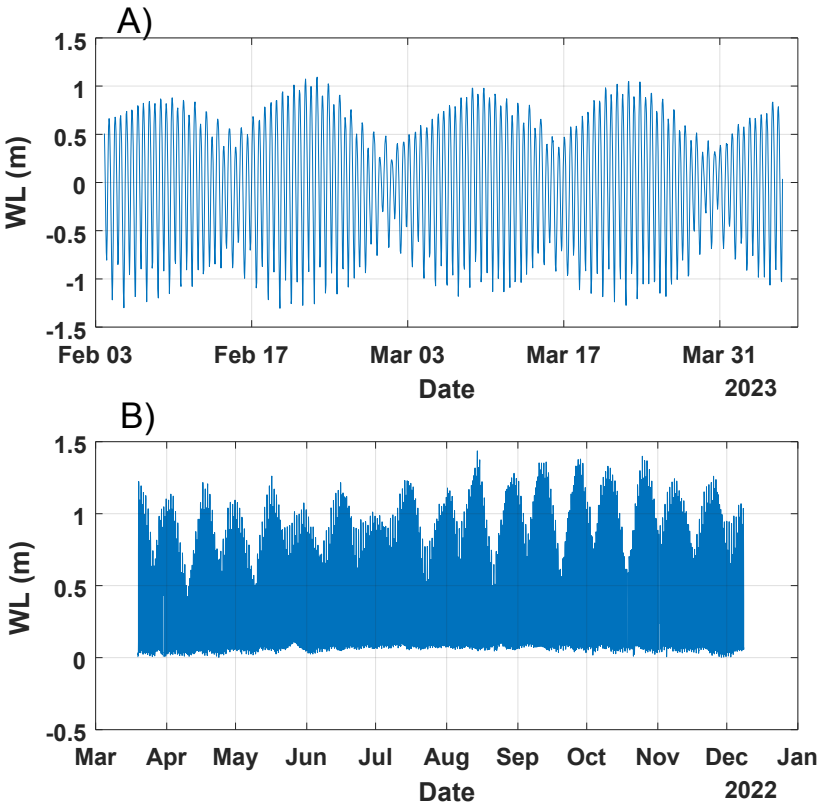

Fig. 2. Water level variations in the Douala basin. A: island sensor. B: Bonassama sensor.

2.3. Ocean tide

Figure 3 shows the WL variations from January 2022 to July 2023 on the ocean side of the constriction zone, off the port of Douala. The tide data was provided to us by the port of Douala, which is responsible for the tide gauge installed on the seaward side of the constriction. This data is acquired every 5 minutes.

While there are interruptions in the observations, a thorough analysis of the time series did not reveal any additional issues, such as vertical repositioning of the tide gauge following an interruption. To fill the missing observations, we used the Pytide software (http://github.com/sam-cox/pytides), which analyzes tidal harmonics by correlating them with the existing signal. The tidal variations closely align with the observations when they are available, resulting in a correlation coefficient of r = 0.89. While some differences exist, they can primarily be attributed to non-tidal and/or high frequency variations, such as the effects of wind. However, these factors are disregarded in this study. The tidal signal observed off the Douala port is semi-diurnal, with a typical amplitude of 1 m but ranging from 0.5 m during neap tides to 1.3 m during spring tides.

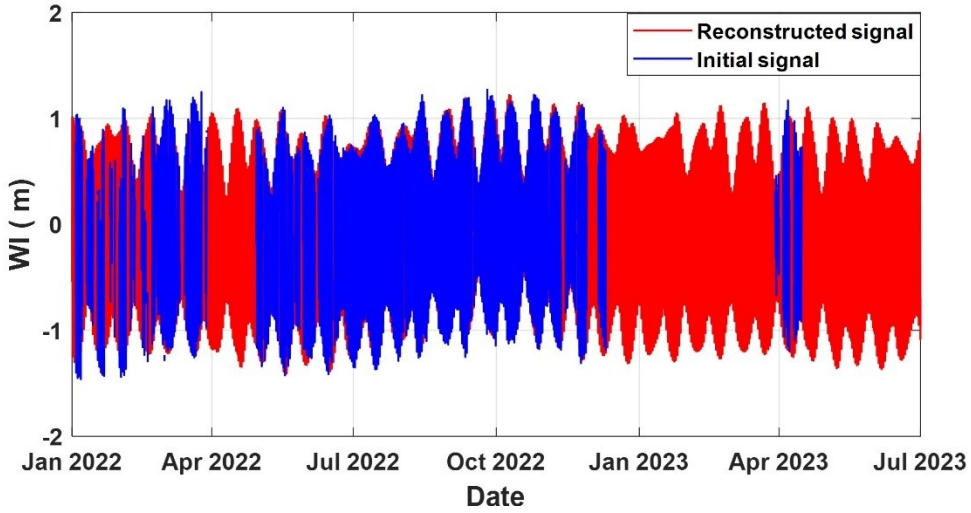

Fig. 3. Water level variations off the Douala port with the reconstructed signal (red), generated using Pytide, superimposed on the observed signal (blue).

2.4. River flow variations

Flash floods in the basin are triggered by sudden increase in river inflow. To analyze the variability of the Wouri River fluxes, we examined 40 years of daily flow data (Olivry, 1974; Tsalefac et al., 2003), from 1951 to 1991 (Figure 4). More recent data are unfortunately not available.

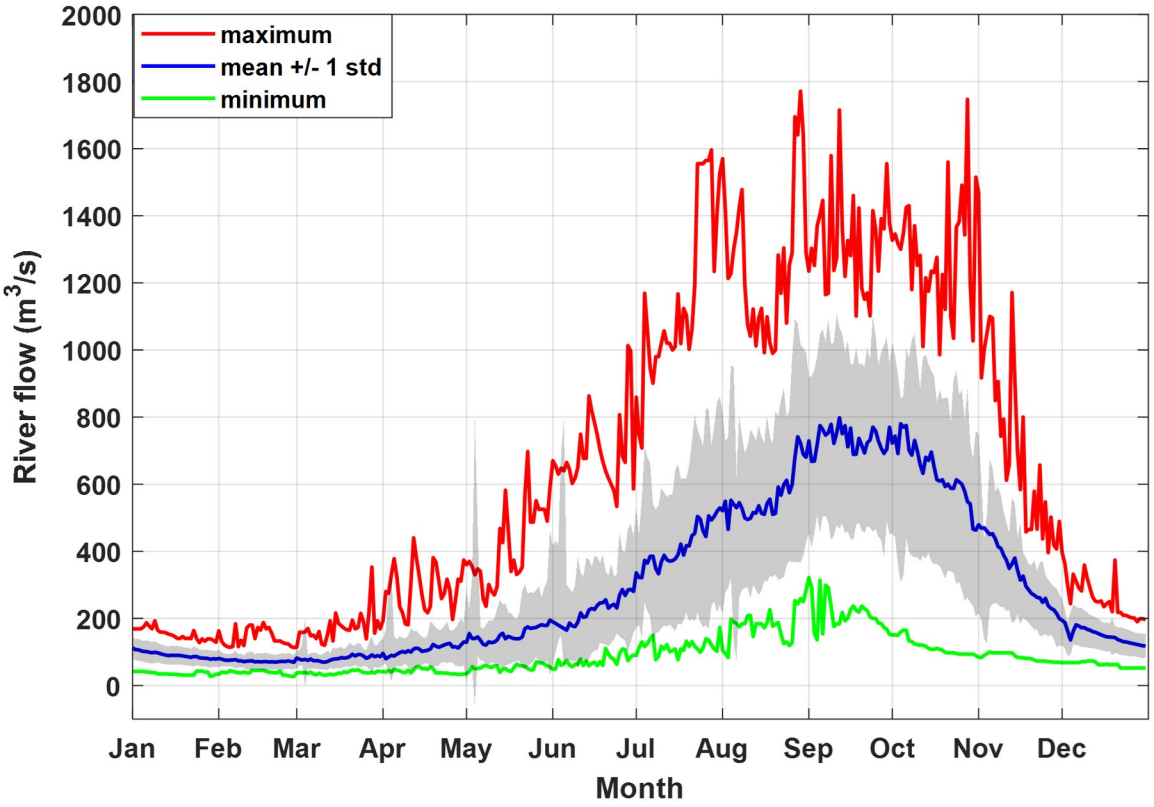

Fig. 4. Mean daily flow of the Wouri River (1951-1991) is shown in blue, with the grey area indicating ± one standard deviation (std) from the mean. Red and green curves represent maximum and minimum daily flows, respectively.

Average maximum flow typically reaches 800 m^3/s, but occasionally the observed flux reaches up to 1800 m^3/s between September and October. Conversely, minimum flux occurring in February and March are about 70 m^3/s.

2.5. Simplified model

Figure 5 depicts the configuration of the theoretical model, which represents the DB connected to the ocean by a constriction (Fig. 1). In the open ocean, sea surface height is mostly controlled by tides, and remains independent of the constriction or basin dynamics and geometry. Conversely, the dynamics within the basin cannot be solely considered as riverine, as its spatial extent and connection to the ocean make the dynamics two-dimensional (2D). However, we consider that WL variations in the sub-basin are predominantly controlled by tides and river inflow, and these variations exhibit relative homogeneity across the entire basin. Thus, we employ a simplified model for basin WL variations based on Stigebrandt (1980) (see also Hill, 1994; MacMahan et al., 2014; Morel et al., 2022). In this model, the constriction controls the exchange between the basin and the open ocean.

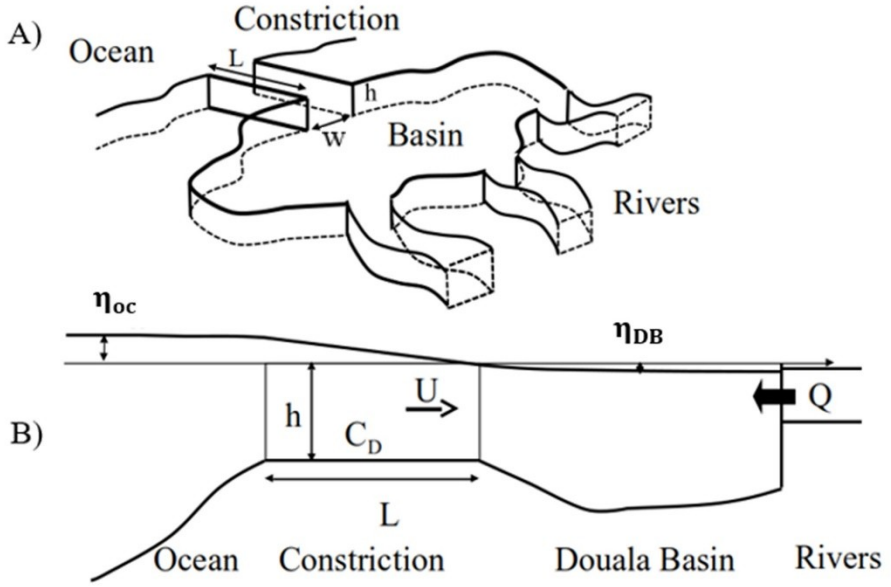

Figure 5: Geometry of the configuration, with a basin connected to the ocean by a channel or constriction and fed by river fluxes. A: general view. B: side view.

The flux in the constriction is hypothesized to be constrained by a balance between the pressure gradient, arising from the WL difference between the ocean and the basin, and bottom friction. This equilibrium can be expressed as:

$$\frac{C_D|U|U}{h} = g\frac{\eta_{oc}-\eta_{DB}}{L} \quad (1)$$

where η_{oc} and η_{DB} are the ocean and basin WL, respectively. g is the gravitational acceleration, L denotes the length of the channel, h is its depth and C_D is the bottom friction coefficient. U represents the mean velocity within the channel, with a positive value indicating flow directed into the basin.

The equation for the basin volume variations is then given by (Stigebrandt, 1980)

$$A\frac{d\eta_{DB}}{dt} = U\,h\,w + Q^{riv} \quad (2)$$

where Q^{riv} is the net river fluxes entering the basin, A is the basin area and w denotes the width of the constriction (Fig. 5-A). Expressing the mean velocity in the channel -U- as a function of the water levels using Eq. 1 and replacing into Eq. 2, we get the final nonlinear equation for η_{DB}

$$\frac{d\eta_{DB}}{dt} = \Gamma \frac{\eta_{oc} - \eta_{DB}}{\sqrt{|\eta_{oc} - \eta_{DB}|}} + \frac{Q^{riv}}{A} \quad (3)$$

Where Γ represents the dissipation or choking coefficient (Stigebrandt, 1980). Theoretically, in very simple configurations and when the water level variations are small in comparison with the channel depth, the combination of Eq. 1 and 2 yields Eq. 3 with $\Gamma \simeq \frac{hw}{A}\sqrt{\frac{gh}{C_D L}}$, so Γ is related to the geometrical characteristics of the constriction and bottom friction (Stigebrandt, 1980). In realistic configurations all characteristics vary within the channel and the latter expression is not valid. However, Γ can be viewed as a coefficient that characterizes the bulk dissipative effects of the constriction and has to be evaluated from observations (Morel et al., 2022). So, we here consider Γ to be constant. To determine its value, we evaluate it using a try/error method. We use Eq. 3, forced by the observed ocean tide and river flux (Fig. 3 and 4), and calculate η_{DB} for various choices of Γ. We then select the value that minimizes the differences with observations. One difficulty in this analysis is the unavailability of the river fluxes for the time period corresponding to the observed basin WL variations (Fig. 2). Consequently, we need to vary both Γ and Q^{riv}. To reduce the number of simulations, we proceed as follows:

- We first focus on the dry season, during which the river flux variations are reduced, using the island η_{DB}observations, which have no bias (Fig. 2A):
    - We use approximate theoretical solutions, valid for low river fluxes and moderate dissipation, to reduce the search interval for Γ values.
    - We apply the try/error method to select the optimal Γ value within this time period.
- We then validate the optimal value for Γ using independent η_{DB}observations at Bonassama, which span both the dry and wet seasons (Fig. 2B).

3. Theoretical solutions

3.1. WL decomposition in the DB

In this section we calculate approximate analytical solutions enabling us to estimate a range of values for the dissipation coefficient Γ from observations of η_{oc} and η_{DB}. We adopt the approach described by Morel et al. (2022), in which we consider a constant river flux and a purely tidal signal in the ocean. Unlike most cases previously studied with the Stigebrandt (1980) model, the tide amplitude in DB is weakly damped. Thus, dissipation in the

constriction is moderate and water level variations in the DB cannot be regarded as small in comparison to the oceanic tide. Morel et al. (2022) hypothesized that the tide variations in the basin are much smaller than in the ocean, but this assumption does not hold in this context. Therefore, it is imperative to develop a new set of solutions considering moderate dissipation. We define

$$\eta_{DB} = \eta_{oc} + \overline{\eta_{DB}} + \tilde{\eta}_{DB} \tag{4}$$

Where $\overline{\eta}_{DB}$ is the mean level in the DB, and $\tilde{\eta}_{DB}$ is the tide modification due to -moderate-dissipation in the constriction and is considered smaller than η_{Oc}: $\tilde{\eta}_{DB} \ll \eta_{oc}$ or $\eta_{DB} \ll \eta_{oc}$. We also assume that $\overline{\eta}_{DB}$ evolves slowly in comparison with the tide period. Note that when there is no tidal variation in the ocean, the mean level is given as the equilibrium between river fluxes and dissipation in the constriction and is $\overline{\eta_{DB}^{riv}}$. Equation 3 shows it is simply given by

$$\overline{\eta_{DB}^{riv}} = \left(\frac{Q^{riv}}{\Gamma A} \right)^2 \tag{5}$$

3.2. *Effect of tidal forcing*

We now consider the ocean sea surface height variations associated with tides. Equation 3 can be rewritten:

$$\overline{\eta_{DB}} + \tilde{\eta}_{DB} = \frac{1}{\Gamma^2} \left(\frac{Q^{riv}}{A} - \frac{\partial \eta_{DB}}{\partial t} \right) \left| \frac{Q^{riv}}{A} - \frac{\partial \eta_{DB}}{\partial t} \right| \tag{6}$$

Given the assumption $\eta_{DB} \ll \eta_{oc}$, we can evaluate a first order correction

$$\overline{\eta_{DB}} + \tilde{\eta}_{DB} = \frac{1}{\Gamma^2} \left(\frac{Q^{riv}}{A} - \frac{\partial \eta_{oc}}{\partial t} \right) \left| \frac{Q^{riv}}{A} - \frac{\partial \eta_{oc}}{\partial t} \right| \tag{7}$$

If we now hypothesize that, over a tide period, η_{oc} can be written with a constant amplitude

$$\eta_{oc} = \delta \eta_{oc} \sin\left(\omega_{M2} t\right) \tag{8}$$

Where $\delta \eta_{oc}$ is the tide amplitude and ω^{M2} is the frequency of the M2 semi- diurnal tide, we get

$$\overline{\eta_{DB}} + \tilde{\eta}_{DB} = \frac{\omega_{M2}^2 \delta \eta_{oc}^2}{\Gamma^2} \left(\frac{Q^{riv}}{A \delta \eta_{oc} \omega_{M2}} - \cos\left(\omega_{M2} t\right) \right) \left| \frac{Q^{riv}}{A \delta \eta_{oc} \omega_{M2}} - \cos\left(\omega_{M2} t\right) \right| \tag{9}$$

which yields

$$\overline{\eta_{DB}} = \frac{\omega_{M2}^2 \delta \eta_{oc}^2}{\Gamma^2} H\left(\frac{Q^{riv}}{A \delta \eta_{oc} \omega_{M2}} \right) \tag{10}$$

where the function H is given by:

$$H(x)=\frac{1}{2\pi}\int_0^{2\pi}(x-\cos(\theta))\left|x-\cos(\theta)\right|d\theta \qquad (11)$$

Equation 9 and 10 can be used to relate $\tilde{\eta}_{DB}$, $\delta\eta_{Oc}$, Γ, Q^{riv} and $\overline{\eta_{DB}}$. During the dry season, river flow is small enough so that Q^{riv} can be neglected when evaluating $\tilde{\eta}_{DB}$ and we finally get the approximate correction

$$\tilde{\eta}_{DB}\simeq\frac{\omega_{M2}^2\delta\eta_{oc}^2}{\Gamma^2}\cos(\omega_{M2}t) \qquad (12)$$

Thus, the amplitude of the tide modification $\tilde{\eta}_{DB}$during the dry season is directly related to the ocean tide amplitude $\delta\eta_{oc}$ and the dissipation parameter Γ. This relation serves as a basis to estimate an interval for Γ values from the observations of $\delta\eta_{oc}$, and $\tilde{\eta}_{DB}$ ($\simeq \eta_{DB}$-η_{oc}) during the dry season.

Note that the previous first order correction (9) or (12) can be reinjected into Eq. (6) to get a second order correction, but this is not of strong interest in the present study.

4. Results

4.1. First estimation of Γ value range

According to our model, Eq. 12 gives a relationship between the oceanic tide amplitude $\delta\eta_{oc}$ and the (slight) modulation of the tidal signal $\tilde{\eta}_{DB} \simeq \eta_{DB}$-$\eta_{oc}$ within the basin. Note that the modified signal is a quadratic phase modulation, meaning it only has a slight impact on the total tide signal.

However, focusing on the amplitude of the modulated signal, Eq. 12 yields

$$\Gamma\simeq\frac{\omega_{M2}\delta\eta_{oc}}{\sqrt{\delta\tilde{\eta}_{DB}}} \qquad (13)$$

where $\delta\tilde{\eta}_{DB}$ is now the amplitude of the modulation and $\omega_{M2}\simeq 1.41\times10^{-4}$ s^{-1}.

We then use the observations of the island sensor and the ocean tide measurements near the port of Douala during a 2-month period in the low water season (see Fig. 2-A), spanning 55 tidal periods.

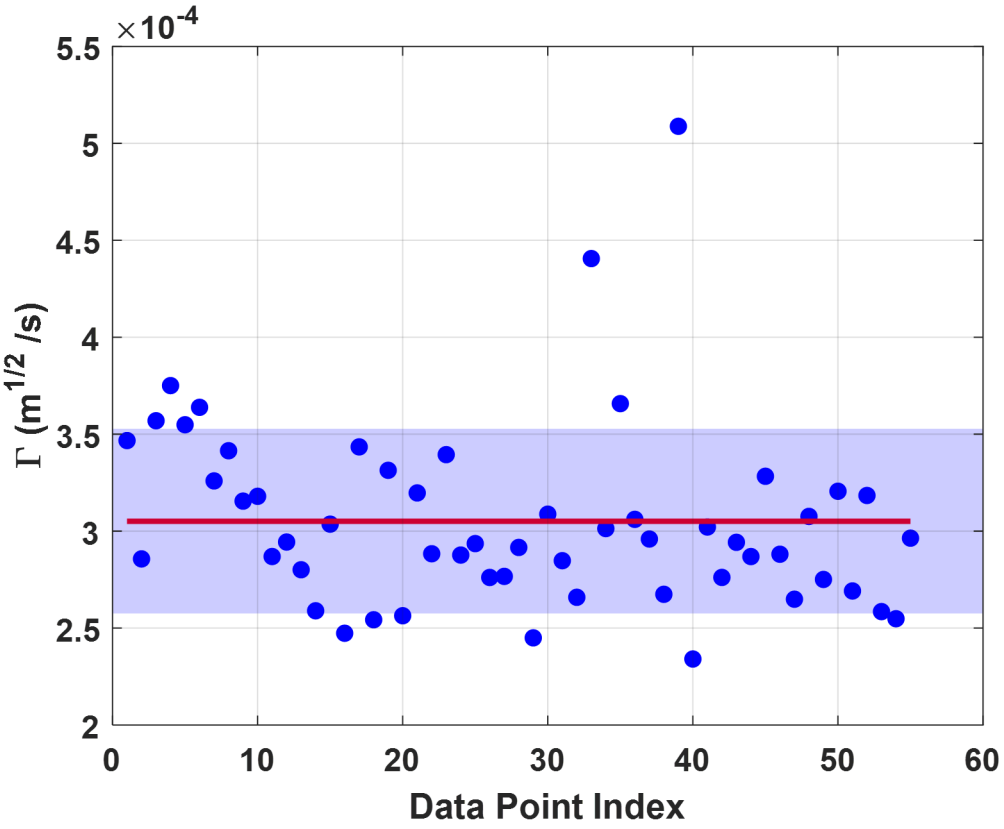

Fig. 6: Γ values for each of the 55 tide periods (data point index). The red line represents the mean value, and the shaded area represents ± one standard deviation from the mean.

We isolate each tidal cycle and estimate both the amplitude of the oceanic tide $\delta\eta_{oc}$ and of the modulated signal amplitude $\delta\tilde{\eta}_{DB}$. From these data, using Eq. 13, we obtained 55 estimates for the dissipation coefficient Γ (Fig. 6). The estimated Γ values vary from 2.3×10^{-4} $m^{1/2}/s$ to 5.1×10^{-4} $m^{1/2}/s$. The mean value is 3.05×10^{-4} $m^{1/2}/s$, the median value is 2.94×10^{-4} $m^{1/2}/s$ and the standard deviation is 4.7×10^{-5} $m^{1/2}/s$.

4.2. Optimal choice for Γ

We now use a try/error method to estimate Γ using WL variations during the time period of the Island sensor observations (February-March). We solve Eq. 3, considering various values for Γ within the range given by Fig. 6 and also varying the river flux Q^{riv} within the range of 70 to 250 m^3/s.

The optimal values resulting in the highest correlation between the observed $\delta\tilde{\eta}_{DB}$at the island sensor and the modeled signal are obtained for Γ = 3×10^{-4} $m^{1/2}/s$ (very close to the estimated

mean Γ in Fig. 6) and Q^{riv} = 150 m^3/s. The phase relationship is generally well represented and follows a quadratic pattern with respect to the oceanic tide forcing (Fig. 7-A), coherent with the approximate theoretical solution (Eq. 12). During spring tides, the amplitudes are very similar. However, during neap tides, some discrepancies appear (Fig. 7-B). Notably, the mean WL differs, and visible modulations are present in the observations, while the model predicts no mean WL variations. It is important to note that the spring tide is of particular interest in this study as it represents the most favorable time period for potential flooding. The correlation of both signals over the entire time period is r = 0.76 with a rmse of 8.5cm. This correlation increases to r = 0.86 with a rmse of 7cm when the analysis is restricted to the spring tide time periods, which is considered satisfactory.

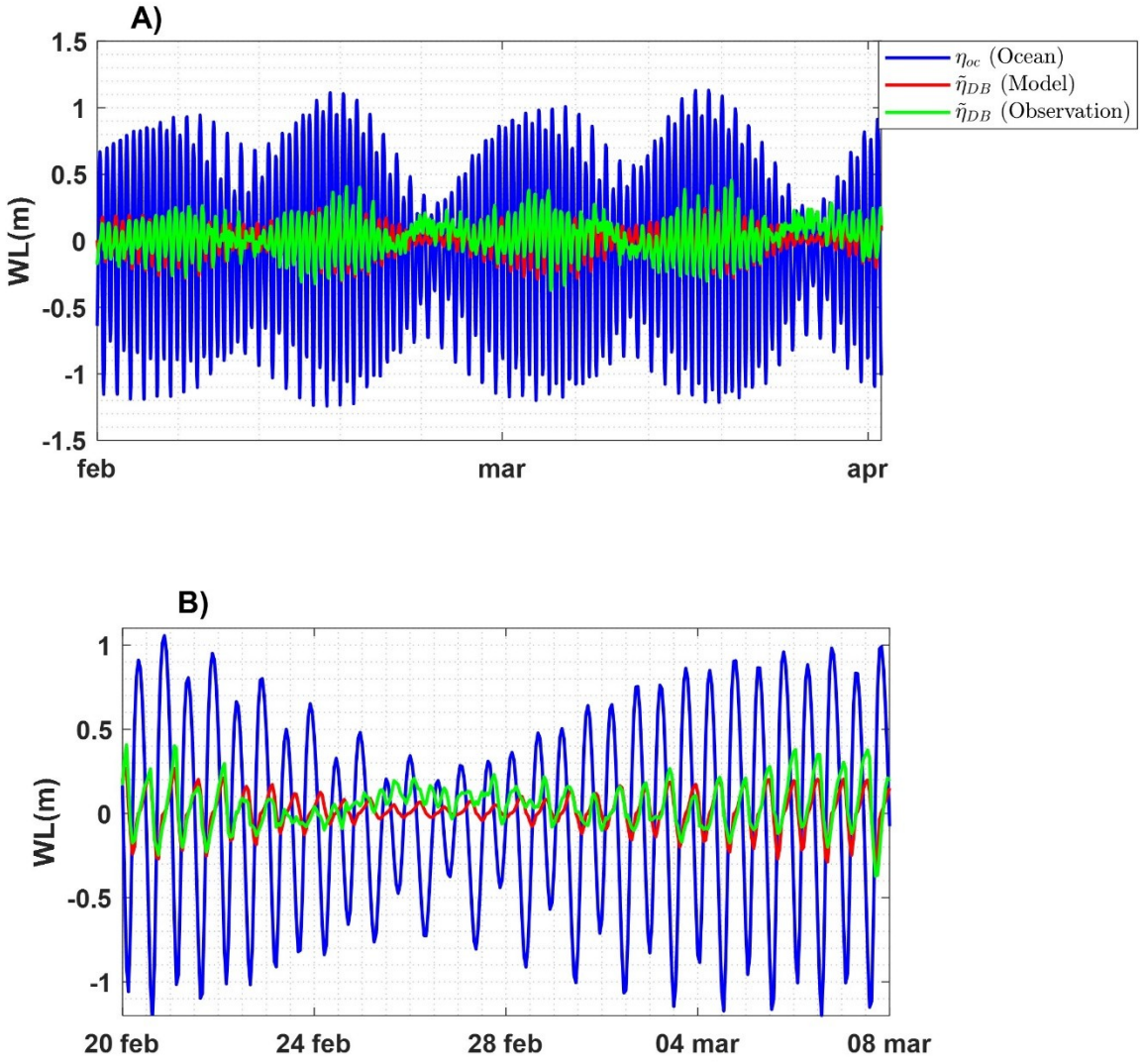

Fig.7. Comparison of the observed (green) and the modeled (red) $\tilde{\eta}_{Db}$ ($\simeq \eta_{Db}$-η_{Oc}) signals in the Douala basin (Island sensor). The blue curve represents the ocean tide. A: for the entire available time series. B: zoom over 16 days from February 20 to March 8.

4.3. Dynamical regime

Theoretical studies evaluating combined effects of river fluxes, tidal forcing and/or wind surge effects in general configurations rely on the use of nondimensional numbers (Stigebrandt, 1980; Hill, 1994; Lorenz, 2023). Two main parameters are useful in the present context.

First, to evaluate the strength of the dissipation, Γ can be non-dimensionalized using the ocean tide amplitude and period. This gives the Stigebrandt choking parameter:

$$P=\frac{2\pi\Gamma}{\omega_{M2}\sqrt{\delta\eta_{oc}}} \quad (14)$$

In the present configuration, we derive a range of P values from 12 to19, corresponding to moderate to small choking or dissipation as expected. Indeed, previous studies have shown that strong choking occurs for P<5 (Stigebrandt, 1980; Hill, 1994).

Another useful parameter is the nondimensional river discharge:

$$S=\frac{2\pi Q^{riv}}{\omega_{M2}A\delta\eta_{oc}} \quad (15)$$

For the present basin, given its relatively small area, the parameter S ranges from 0.2 to 3 for mean (climatic) seasonal variations and can reach 7 for extreme river flows (Q^{riv}= 1800 m^3/s). This corresponds to strong river discharge regimes.

Moderate tidal dampings have been observed and studied in other estuaries (e.g., Guo et al., 2015; Jalón-Rojas et al., 2017; 2018; Cai et al, 2018; Xie et al., 2022), but to our knowledge the combination of moderate dissipation and strong river flow has been seldom addressed (Stigebrandt, 1980; Lorenz, 2023). The combination of moderate to small choking with strong river flow is thus an interesting regime, worth studying as it corresponds to many lagoon or basin along the Western Africa coast.

4.4. Validation of the DB WL model

To further validate the model during a period of strong river fluxes, we conduct simulations for the time period corresponding to the Bonassama observations, using $\Gamma = 3\times10^{-4}$ $m^{1/2}/s$. Since river flow data are not available for the study period, we use the mean historical flow data presented previously. As the available observations at Bonassama are cut off at low tide, we use the maximum values of the WL averaged over March and April to define a reference level so that the maximum levels observed coincides with the model (for which the variations are relative to the mean sea level).

Figure 8 represents the comparison between the observations (green curve) and the model (red curve) for the entire duration of the Bonassama observations (Fig. 8-A) and for a restricted time period in late August-early September (Fig. 8-B), when the river fluxes are near their maximum (~800 m^3/s). The correlation between the observed WL and the model (excluding threshold observations) is satisfying with an r = 0.79. We now focus on the maximum WL reached during each tide cycle throughout the entire observation period (Fig. 8-C), which is of major interest for flooding considerations. The maximum amplitudes closely align throughout the entire period and show a remarkably high correlation at r = 0.94 and a rmse of 7 cm. While some discrepancies of up to 20 cm are observed in the dry season, these can be attributed to the specific choice of river flow, which was made on an ad hoc basis. Overall, we consider the performance of the model adapted to the requirements of this study.

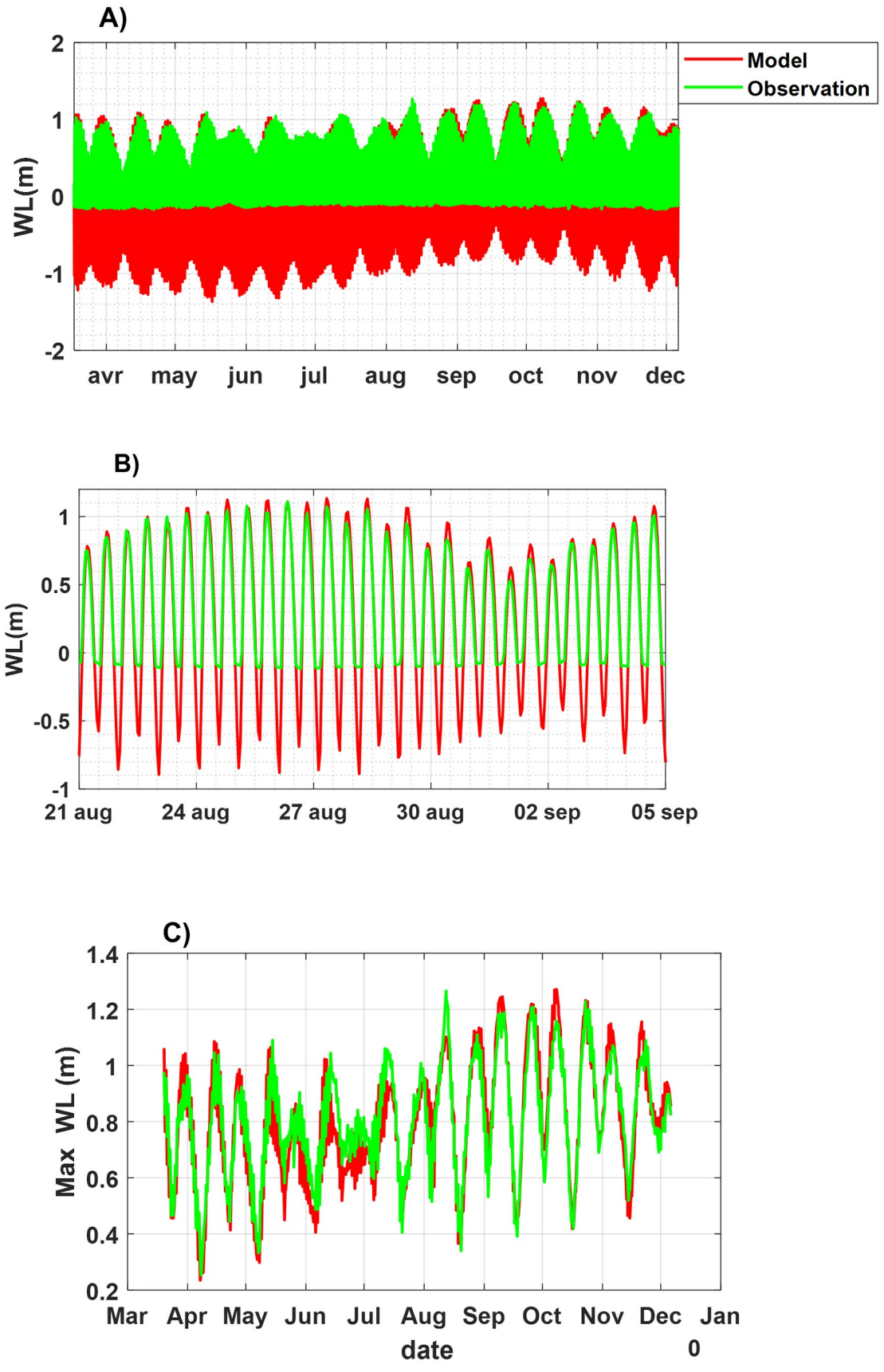

Fig. 8. A: comparison between observed (green) and simulated (red) WL variation at Bonassama. B: zoom over 15 days from August 21 to September 5. C: maximum WL evolution.

4.5. *WL and tide amplitude in the DB*

We now evaluate the mean WL and tidal amplitude in the Douala basin across a range of values of river flux and ocean tide amplitude. For the rest of the study, we concentrate on the Douala basin. We thus again set $\Gamma = 3\times10^{-4}$ $m^{1/2}/s$, we vary the tide amplitude from 0.3 to 1.5 m and the river flow from 0 to 3000 m^3/s. Given the previous characteristics, the nondimensional parameter P (Eq. 14) varies from 12 to 19 and S (Eq. 15) varies from 0 to 12, a combination that is rarely studied. We solve Eq. 3 over ten M2 tide periods and for the chosen values of Q^{riv}, $\delta\eta_{oc}$ and the calculated value for Γ. This time period is sufficiently long so that a stationary state is reached (the WL has regular oscillations around a constant mean) and we use the last M2 period to evaluate the mean WL and tide amplitude in the basin.

Figure 9 represents the combined influence of river flow and ocean tide amplitude $\delta\eta_{oc}$, on the mean WL of the Douala basin $\overline{\eta_{DB}}$ (Fig. 9-A). The effect of tides on the mean WL is obtained by subtracting $\overline{\eta_{DB}^{riv}}$ (given by Eq. 5) and is represented in Fig.9-B. As expected, WL consistently increases with tidal amplitude (e.g., Morel et al., 2022). The maximum increase due to tides is reached for intermediate river fluxes, specifically in the range of Q^{riv} = 500 m^3/s to 1500 m^3/s within the considered tidal range. Notably, the mean WL remains below 0.5 m if $Q^{riv} \leq 2000 m^3/s$ but increases quadratically.

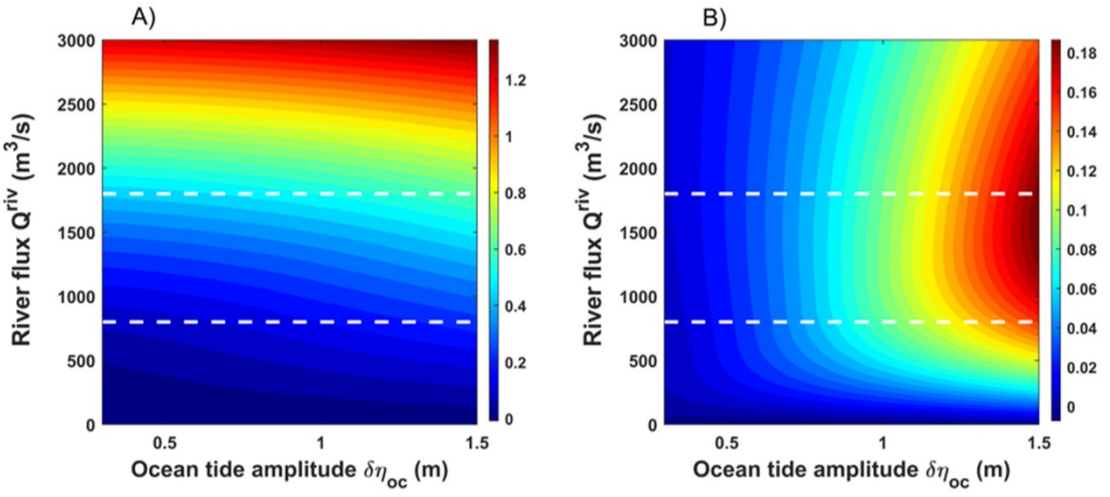

Fig. 9. A: mean WL in the Douala basin depending on river flow and ocean tide. B: increase in mean WL due to tide. The white dotted lines represent the maximum of the average climatological year (800

m^3/s) and the absolute maximum (1800 m^3/s) for the observed river flow. The results are obtained with $\Gamma = 3\times10^{-4}$ $m^{1/2}/s$ (giving nondimensional parameter ranges P=12 to 19 and S=0 to 12, see Eq. 14 and 15).

Figure 10 represents the tide amplitude in the basin $\delta\eta_{DB}$ (Fig. 10-a) and its variation with respect to ocean tide (Fig. 10-B). The tide amplitude in Douala basin is always below the oceanic one, indicating the tidal choking effect of the constriction (Stigebrandt, 1980, 1992). It is important to note that this damping effect intensifies with both ocean tide amplitude and river flow.

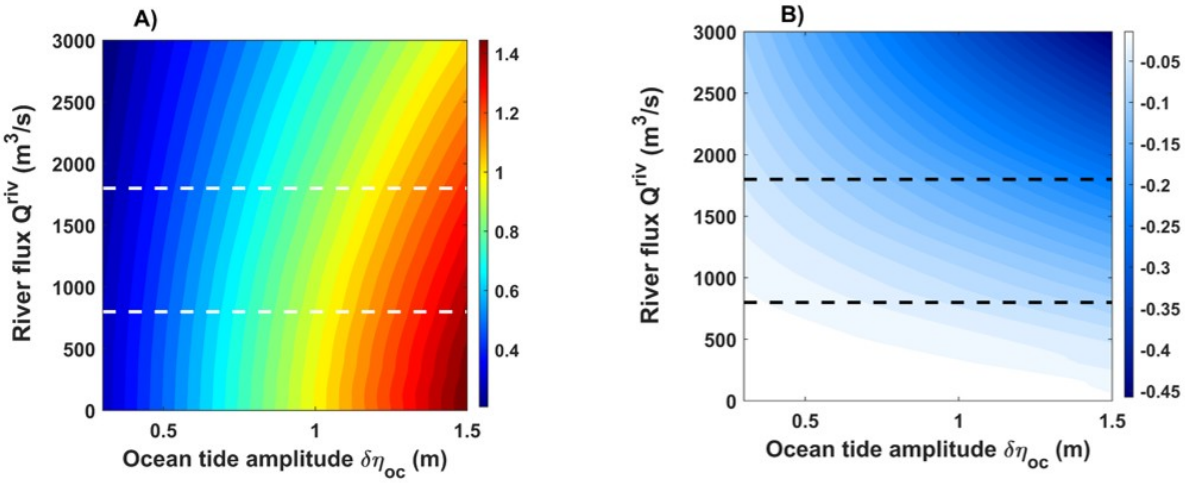

Fig. 10. Tide amplitude in the Douala basin as a function of river flow and ocean tide. A: tide amplitude. B: tidal amplitude damping (difference between the amplitude in the basin and the ocean tide). The white and black dotted lines represent the maximum of the average climatological year (800 m^3/s) and the absolute maximum (1800 m^3/s) for the observed river flow. The results are obtained with $\Gamma = 3\times10^{-4}$ $m^{1/2}/s$ (giving nondimensional parameter ranges P=12 to 19 and S=0 to 12, see Eq. 14 and 15).

5. Discussion

5.1. Maximum WL in Douala basin due to tide and river flow

There are two counteracting effects of the constriction on the WL in the Douala basin: as the river flux increases, it increases the mean WL but decreases the tidal amplitude. The maximum WL that can be reached in the Douala basin is represented in Fig. 11. It is close to

the sum of the mean WL and tide amplitude (because of dissymmetries between the flood and ebb tide phases, the maximum water level is not equal to the sum of the mean level and tide amplitude). With respect to future scenarios, the ocean tide is expected to remain relatively stable, but river flux can be modified which will potentially impact the maximum WL in the basin.

Given the lack of precise and georeferenced topographies of Douala city, in particular near the estuary, establishing thresholds for flooding is challenging. However, based on our own field estimates, we believe that a surge (an increase of level in comparison with the maximum tide amplitude in the basin) of about 0.5 m is enough to flood some suburbs along the western side of the basin. To inundate the eastern side, at least a 1 m surge is deemed necessary. This criterion is applied in the subsequent analysis.

It is first worth noting that on long term average, the mean maximum river flow is $Q^{riv} \simeq 800 m^3/s$ (lower white dotted in Fig. 11), and the maximum water level in the Douala basin remains close to the oceanic tide amplitude; the surge above the basin tide induced by river input remains below 0.2 m (see Fig. 9). Even at maximum river flow $Q^{riv} \simeq 1800 m^3/s$ (2nd white dotted line in Fig. 11), the maximum WL in the basin is about 1.7 m, equivalent to a surge of 0.7 m above the basin tide (Fig. 9). Such a surge is sufficient to cause minor flooding in the low-lying areas bordering the western side of the Douala basin, but it cannot account for the severe floods experienced in the topographically higher Douala city on the eastern side of the basin. Thus, recent floods in the city must be attributed to other mechanisms, such as local watershed dynamics associated with small rivers passing through Douala city (Tongo Basa in particular, Iroume et al, 2022; Essoh et al, 2023). In some future climate change scenarios, the average Monsoon rainfall is predicted to increase by about 20% or more (Trisos et al., 2022). It is also conceivable that extreme rainfall events may become more intense. Our model suggests that, for river fluxes of $2500 m^3/s$, the WL will reach 2.1m, with the flood-driven surge still remaining below 1 m with respect to the basin tide. However, if the Wouri river flow was to reach $Q^{riv} \simeq 3000 m^3/s$, the surge could potentially reach 1.3m. Such an increase would lead to more severe floods on the western side and could also impact Douala city on the eastern side of the basin. Finally, in the present study and discussion, we focused on the effect of river flow, but other processes can play a role on the maximum WL reached in the Douala basin and are discussed in the concluding section.

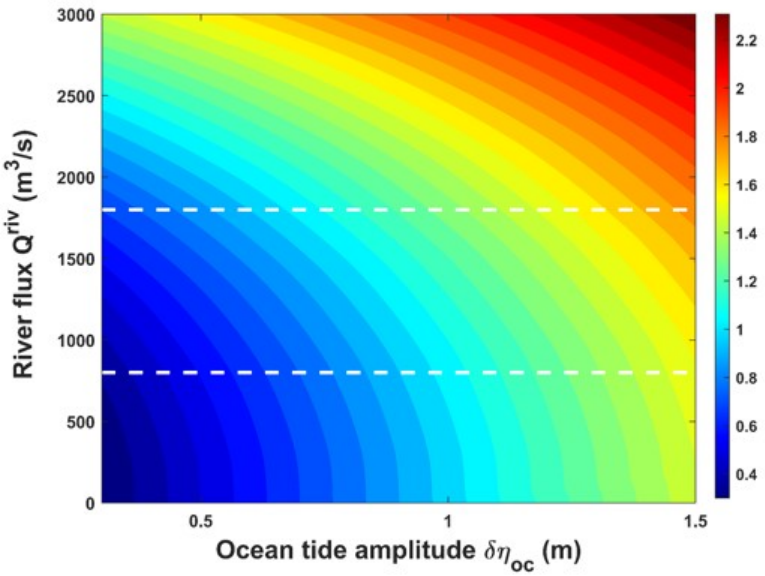

Fig. 11. Maximum water level reached in the Douala basin as a function of the Wouri outflow and oceanic tide amplitude. The dotted lines indicate the 800m^3/s (mean long-term maximum river flow) and 1800m^3/s (maximum river flow observed during in the 1951-1991 period) flow rates. The results are obtained with $\Gamma = 3\times10^{-4}$ $m^{1/2}$/s (giving nondimensional parameter ranges P=12 to 19 and S=0 to 12, see Eq. 14 and 15).

5.2. Limitations of the present study and further analyses

While our model has demonstrated its effectiveness in accurately representing maximum water level variations over a complete seasonal cycle (as shown in Fig. 8-C), it is important to acknowledge certain assumptions and approximations that underlie the model. Firstly, the determination of the dissipation parameter Γ plays a pivotal role in our calculations. The estimation of Γ is associated with uncertainty up to 15% (Fig. 6). This uncertainty can probably be reduced because it is most likely associated with high frequency processes induced by the wind or river flux.

A major limitation is the lack of recent river flow data for the Wouri, with the latest available data dating back to the early 1990s. Consequently, the discussion regarding the effect of climate change on river flow remains speculative at this stage. Continuous monitoring of this river is important to obtain more reliable estimates of potential WL variations in the future.

Lastly, our estimates for tide amplitude, mean WL and maximum WL variations as a function of oceanic tide amplitude and river flow are based on an equilibrium state, assuming

regular tides and constant river flow. If river flow varies, especially reaching peak levels over a limited time period, our model may overestimate the mean and maximum WL. However, as described in Section 2.5, our model can be adapted to accommodate variable river flows. This adaptation could help estimate the typical timescale over which river flow variability can be neglected. We can derive an exact solution for a configuration where the WL is initially at zero and a river flux Q^{riv} is suddenly applied at $t = 0$. Neglecting oceanic tide, since we want to estimate the adjustment time period associated with an increase in river flow, the WL at equilibrium is $\overline{\eta_{DB}^{riv}}$ (given by Eq. 5). Equation 3 then becomes

$$\frac{d\eta_{DB}}{dt} = -\Gamma\sqrt{\eta_{DB}} + \frac{Q^{riv}}{A} \tag{16}$$

which can be integrated to give a relationship between time and the WL η_{DB}

$$t = \frac{-2}{\Gamma}\left[\sqrt{\eta_{DB}} + \frac{Q^{riv}}{\Gamma A}\ln\left(1 - \frac{\sqrt{\eta_{DB}}}{Q^{riv}/\Gamma A}\right)\right] \tag{17}$$

Taking advantage of the definition of $\overline{\eta_{DB}^{riv}}$ (Eq. 5), this can be written

$$t = \frac{-2Q^{riv}}{\Gamma^2 A}\left[\sqrt{\frac{\eta_{DB}}{\eta_{DB}^{riv}}} + \ln\left(1 - \sqrt{\frac{\eta_{DB}}{\eta_{DB}^{riv}}}\right)\right] \tag{18}$$

The equilibrium value can be considered reached when

$\sqrt{\eta_{DB}} \simeq 0.99\sqrt{\overline{\eta_{DB}^{riv}}}$ and the adjustment timescale is thus given by

$$T_{adj} = \frac{-2Q^{riv}}{\Gamma^2 A}\left[0.99 + \ln(1 - 0.99)\right] \simeq 7\frac{Q^{riv}}{\Gamma^2 A} \tag{19}$$

For the Douala basin, for the estimated Γ value and the given basin area, the adjustment timescale to reach equilibrium for an increase of river flow of Q^{riv} = 1000 m^3/s is $T_{adj} \simeq 20$ min. In practice, this is small enough to consider equilibrium (and the highest level) is systematically reached in the Douala basin, as assumed here.

6. Conclusion

This study allows to dissociate the effects of ocean tides and river flow in a coastal/estuarine basin with a significant flow constriction. At current river flow conditions, floods along the western side of the basin can be explained by interacting tides and river flow,

but severe flooding within Douala city cannot be attributed to surges from the Douala basin. Our study indicates that, presently, only extreme river flows, exceeding 3000 m^3/s, may result in inundation of Douala city originating from the Wouri basin. Such extreme flows have never been observed and remain unlikely. However, in addition to modifying river flows, climate change will also result in a sea level rise of approximately 30 cm by the end of the century (Cazenave and Cozannet, 2014; Fossi Fotsi et al., 2019). This elevation of the mean ocean level will lower the threshold for flooding to about 0.7 m which can be much more easily achieved and, in addition to the combined effect of ocean tide and river flow, other processes can become important.

The wind is known to cause significant WL fluctuations in some lagoons, often associated with seiche events (e.g., Chaigneau et al., 2022). Lorenz et al (2023) have extended Stigebrandt model to take into account wind stress, which could be useful for the present configuration, provided local wind can be observed/estimated. Given the limited size of the Douala basin, seiche amplitudes should remain relatively modest, likely in the range of few centimeters. However, even such a moderate surge could become significant in the context of climate change.

In specific tidal estuaries or basins, sediment inputs from rivers combined with complex dynamics have been documented to induce bathymetric alterations, thereby influencing water level variations (Hoitink et al, 2017; Xie et al., 2017; 2018; 2022, Wu et al, 2020), a process that we have neglected here. Bathymetric data acquired both before and after flood events, or measurements of sediment stability, are of interest to evaluate bathymetry evolution. In the long term, recent studies have shown significant accretion along the coastline of the constriction (Fossi Fotsi et al, 2019). A narrowing or maximum depth reduction of the constriction could have drastic consequences on its dissipation characteristics, and subsequently on the maximum WL that can be reached in the basin. Finally, the combination of different effects discussed above, such as bathymetric and basin area changes, along with the modification of river flow could lead to enhanced impacts (Lorenz et al, 2023).

Our simplified model did not incorporate additional factors such as groundwater inputs, smaller river inputs, high- frequency variations in ocean level (related to coastal waves, wind effect or large-scale circulation on coastal WL) and evaporation. While these parameters may have some impacts on Douala basin WL, their effects are expected to be limited and are unlikely to alter our overall conclusions for the present conditions. However, they can become significant if climate change drastically modifies the geomorphology of the estuary.

A major challenge we encountered in our study, which is a common issue in African

countries, is the lack of recent river flow data. While we use historic river flow rates in our study, they may not accurately represent present conditions. It is crucial to monitor the Wouri River flow to assess recent and future changes and validate the river flow range used in our study. Satellite altimetric missions, such as the recent SWOT mission, hold promise for providing virtual gauges for rivers worldwide, facilitating effective river flow monitoring and flood warning systems. Finally, precise georeferenced topographic data of the city bordering the basin would also help determine more precise thresholds for flooding.

Acknowledgements.

W. N. DIMA was funded through a scholarship grant of the German Academic Exchange Service DAAD (Deutscher Akademischer Austauschdientst) within the framework of the "In-Country/In-Region Scholarship Program" for sub-Saharan Africa. The study also benefited from financial support from IRD (Institute of Research for Development). We would like to sincerely thank the people who participated in the deployment and recovery of the sensors.

We also express our gratitude to LANGOUL Ulrich and AWOULMBANG SAKPAK Thierry Derol for their assistance in acquiring certain data.

The manuscript also benefited from the corrections and suggestions of 2 anonymous reviewers: their careful reading and many ideas have significantly improved the quality of the document.

References

Abebe, Y., Kabir, G., & Tesfamariam, S. (2018). Assessing urban areas vulnerability to pluvial flooding using GIS applications and Bayesian Belief Network model. Journal of Cleaner Production, 174, 1629-1641.

Albrecht, N., & Vennell, R. (2007). Tides in two constricted New Zealand lagoons. New Zealand Journal of Marine and Freshwater Research, 41(1), 103-118.

Amanejieu, A. (2018). End of study work: "temporal analysis of the representation of flood risk from 1980 to 2018 in douala-cameroon".

Barbone, E., & Basset, A. (2010). Hydrological constraints to macrobenthic fauna biodiversity in transitional waters ecosystems. Rendiconti Lincei, 21, 301-314.

Bertoni, J.C. (2006). Urban flooding in Latin America: reflections on the role of risk factors. IAHS-AISH publication, 123-141.

Besack, Felix & Onguéné, Raphaël & Rodrigue, Ebonji & Lawrence, Oben & Betsaleel, Kouandji & Willy, Sone & Eyango, M. (2020). Small Scales Dynamics Inferred from Tidal Measurements to Mitigate Daily Floodings in the City of Douala: A Case Study of the Besseke's Flood Drain. Journal of Geography, Environment and Earth Science International. 45-62. 10.9734/jgeesi/2020/v24i130193.

Bruckmann, L., Amanejieu, A., Moffo, M. O. Z., Ozer, P., 2019. Geohistorical analysis of the spatio-temporal evolution of flood risk and its management in the urban area of Douala (Cameroon). Physio-Geo. Physical geography and environment (Volume 13), 91–113.

Buschman, F. A., Hoitink, A. J. F., Van Der Vegt, M., & Hoekstra, P. (2009). Subtidal water level variation controlled by river flow and tides. Water Resources Research, 45(10).

Cai, H., Yang, Q., Zhang, Z., Guo, X., Liu, F., & Ou, S. (2018). Impact of river-tide dynamics on the temporal-spatial distribution of residual water level in the Pearl River channel networks. *Estuaries and Coasts*, *41*, 1885-1903.

Cazenave, A., & Cozannet, G. L. (2014). Sea level rise and its coastal impacts. Earth's Future, 2(2), 15-34.

Chaigneau, A., Okpeitcha, O. V., Morel, Y., Stieglitz, T., Assogba, A., Benoist, M., ... & Sohou, Z. (2022). From seasonal flood pulse to seiche: Multi-frequency water-level fluctuations in a large shallow tropical lagoon (Nokoué Lagoon, Benin). Estuarine, Coastal and Shelf Science, 267, 107767.

Duck, R. W., & da Silva, J. F. (2012). Coastal lagoons and their evolution: A hydromorphological perspective. Estuarine, Coastal and Shelf Science, 110, 2-14.

Essoh, W. S., Onguene, R., Ndongo, B., Nshagali, G., Colmet-Daage, A., Marie, G., ... & Braun, J. J. (2023). Using GIS and Multicriteria Analysis to Map Flood Risk Areas of the Tongo Bassa River Basin (Douala, Cameroon). *Journal of Coastal Research*, *39*(3), 531-543.

Fossi Fotsi, Y., Pouvreau, N., Brenon, I., Onguene, R., & Etame, J. (2019). Temporal (1948–2012) and dynamic evolution of the Wouri estuary coastline within the Gulf of Guinea. Journal of Marine Science and Engineering, 7(10), 343.

Fossi Fotsi, Y., Brenon, I., Pouvreau, N., Ferret, Y., Latapy, A., Onguene, R., Jombe, D & Etame, J. (2023). Exploring tidal dynamics in the Wouri estuary, Cameroon. Continental Shelf Research, 104982.

Glenne, B., & Simensen, T. (1963). Tidal current choking in the landlocked fjord of NordÅsyatnet. Sarsia, 11(1), 43-73.

Gonenc, I. E., & Wolflin, J. P. (Eds.). (2004). Coastal lagoons: ecosystem processes and modeling for sustainable use and development. CRC Press.

Guo, L., van der Wegen, M., Jay, D. A., Matte, P., Wang, Z. B., Roelvink, D., & He, Q. (2015). River-tide dynamics: Exploration of nonstationary and nonlinear tidal behavior in the Yangtze River estuary. *Journal of Geophysical Research: Oceans*, *120*(5), 3499-3521.

Harley, C. D., Randall Hughes, A., Hultgren, K. M., Miner, B. G., Sorte, C. J., Thornber, C. S., ... & Williams, S. L. (2006). The impacts of climate change in coastal marine systems. Ecology letters, 9(2), 228-241.

Hill, A. E. (1994). Fortnightly tides in a lagoon with variable choking. Estuarine, Coastal and Shelf Science, 38(4), 423-434.

Hoitink, A. J. F., Wang, Z. B., Vermeulen, B., Huismans, Y., & Kästner, K. (2017). Tidal controls on river delta morphology. *Nature geoscience*, *10*(9), 637-645.

Hu, M., Zhang, X., Li, Y., Yang, H., & Tanaka, K. (2019). Flood mitigation performance of low impact development technologies under different storms for retrofitting an urbanized area. Journal of Cleaner Production, 222, 373-380.

Jalón-Rojas, I., Schmidt, S., & Sottolichio, A. (2017). Comparison of environmental forcings affecting suspended sediments variability in two macrotidal, highly-turbid estuaries. *Estuarine, Coastal and Shelf Science*, *198*, 529-541.

Jalón-Rojas, I., Sottolichio, A., Hanquiez, V., Fort, A., & Schmidt, S. (2018). To what extent multidecadal changes in morphology and fluvial discharge impact tide in a convergent (turbid) tidal river. *Journal of Geophysical Research: Oceans*, *123*(5), 3241-3258.

Junior Yves-Audrey Iroume, Raphaël Onguéné, Francis Djanna Koffi, Antoine Colmet-Daage, Thomas Stieglitz, et al. The 21st August 2020 Flood in Douala (Cameroon): A Major Urban Flood Investigated with 2D HEC-RAS Modeling. Water, 2022, 14, ff10.3390/w14111768ff. ffird-03761838

MacMahan, J., van de Kreeke, J., Reniers, A., Elgar, S., Raubenheimer, B., Thornton, E., ... & Brown, J. (2014). Fortnightly tides and subtidal motions in a choked inlet. Estuarine, Coastal and Shelf Science, 150, 325-331.

Lorenz, M., Arns, A., & Gräwe, U. (2023). How sea level rise may hit you through the backdoor: Changing extreme water levels in shallow coastal lagoons. Geophysical Research Letters, 50(21), e2023GL105512.

Maicu, F., Abdellaoui, B., Bajo, M., Chair, A., Hilmi, K., & Umgiesser, G. (2021). Modelling the water dynamics of a tidal lagoon: The impact of human intervention in the Nador Lagoon (Morocco). *Continental Shelf Research*, *228*, 104535.

Martinis, S. (2017, July). Improving flood mapping in arid areas using Sentinel-1 time series data. In *2017 IEEE international geoscience and remote sensing symposium (IGARSS)* (pp. 193-196). IEEE.

Morel, Y., Chaigneau, A., Okpeitcha, V. O., Stieglitz, T., Assogba, A., Duhaut, T., ... & Sohou, Z. (2022). Terrestrial or oceanic forcing? Water level variations in coastal lagoons constrained by river inflow and ocean tides. *Advances in Water Resources*, *169*, 104309.

Munji, C. A., Bele, M. Y., Idinoba, M. E., & Sonwa, D. J. (2014). Floods and mangrove forests, friends or foes? Perceptions of relationships and risks in Cameroon coastal mangroves. *Estuarine, Coastal and Shelf Science*, *140*, 67-75.

Newton, A., Brito, A. C., Icely, J. D., Derolez, V., Clara, I., Angus, S., ... & Khokhlov, V. (2018). Assessing, quantifying and valuing the ecosystem services of coastal lagoons. *Journal for Nature Conservation*, *44*, 50-65.

Oliveira, A. M., & Kjerfve, B. (1993). Environmental responses of a tropical coastal lagoon system to hydrological variability: Mundau-Manguaba, Brazil. *Estuarine, Coastal and Shelf Science*, *37*(6), 575-591.

Olivry, J., 1974. Hydrological regime of the Wouri river and estimation of the contributions received by the Wouri estuary and mangrove. Overseas Scientific and Technical Research Office, ORSTOM. United Republic of Cameroon.

Paprotny, D., Sebastian, A., Morales-Nápoles, O., & Jonkman, S. N. (2018). Trends in flood losses in Europe over the past 150 years. *Nature communications*, *9*(1), 1985.

Sassi, M. G., & Hoitink, A. J. F. (2013). River flow controls on tides and tide-mean water level profiles in a tidal freshwater river. *Journal of Geophysical Research: Oceans*, *118*(9), 4139-4151.

Scanes, E., Scanes, PR and Ross, PM (2020). Climate change is rapidly warming and acidifying Australian estuaries. Natural Communications, 11 (1), 1803.

Speer, P. E., & Aubrey, D. G. (1985). A study of non-linear tidal propagation in shallow inlet/estuarine systems Part II: Theory. *Estuarine, Coastal and Shelf Science*, *21*(2), 207-224.

Stigebrandt, A. (1980). Some aspects of tidal interaction with fjord constrictions. *Estuarine and Coastal Marine Science*, *11*(2), 151-166.

Stigebrandt, A. (1992). Bridge-induced flow reduction in sea straits with reference to effects of a planned bridge across Öresund. *Ambio*, 130-134.

Stocker, T. (Ed.). (2014). *Climate change 2013: the physical science basis: Working Group I contribution to the Fifth assessment report of the Intergovernmental Panel on Climate Change*. Cambridge university press.

Tagliapietra, D., Sigovini, M., & Ghirardini, A. V. (2009). A review of terms and definitions to categorise estuaries, lagoons and associated environments. *Marine and freshwater Research*, *60*(6), 497-509.

Trisos, C., Adelekan, I., Totin, E., Ayanlade, A., Efitre, J., Gemeda, A., Kalaba, K., Lennard, C., Masao, C., Mgaya, Y., Ngaruiya, G., Olago, D., Simpson, N., Zakieldeen, S., 2022. Africa. Cambridge University Press, Cambridge, UK and New York, USA, pp. 1285–1455.

Tsalefac, M., Ngoufo, R., Nkwambi, W., Tatsangue, E. D., Fobissie, B. L., 2003. Frequencies and quantities of daily precipitation on Cameroonian territory. Publ. AIC 15, 359–367.

Umgiesser, G., Ferrarin, C., Cucco, A., De Pascalis, F., Bellafiore, D., Ghezzo, M., & Bajo, M. (2014). Comparative hydrodynamics of 10 Mediterranean lagoons by means of numerical modeling. *Journal of Geophysical Research: Oceans*, *119*(4), 2212-2226.

Viaroli, P., Lasserre, P., & Campostrini, P. (2007). Lagoons and coastal wetlands in the global change context: impacts and management issues. *Hydrobiologia*, *577*, 1-168.

Wilson, G. V., Rigby, J. R., Ursic, M., & Dabney, S. M. (2016). Soil pipe flow tracer experiments: 1. Connectivity and transport characteristics. *Hydrological Processes*, *30*(8), 1265-1279.

Wu, Y., He, Y., Lu, C., Zhang, W., & Gao, S. (2020). Feedback between channel resilience and tidal dynamics in an intensively dredged tidal river. *Journal of Hydrology*, *590*, 125367.

Xie, D., Gao, S., Wang, Z. B., Pan, C., Wu, X., & Wang, Q. (2017). Morphodynamic modeling of a large inside sandbar and its dextral morphology in a convergent estuary: Qiantang Estuary, China. *Journal of Geophysical Research: Earth Surface*, *122*(8), 1553-1572.

Xie, D., Pan, C., Gao, S., & Wang, Z. B. (2018). Morphodynamics of the Qiantang Estuary, China: Controls of river flood events and tidal bores. *Marine Geology*, *406*, 27-33.

Xie, D., Wang, Z. B., Huang, J., & Zeng, J. (2022). River, tide and morphology interaction in a macro-tidal estuary with active morphological evolutions. *Catena*, *212*, 106131.

Zheng, F., Westra, S., & Sisson, S. A. (2013). Quantifying the dependence between extreme rainfall and storm surge in the coastal zone. *Journal of Hydrology*, *505*, 172-187.